

Document downloaded from:

<http://hdl.handle.net/10251/119397>

This paper must be cited as:

Robles Martínez, Á.; Capson-Tojo, G.; Ruano García, MV.; Seco Torrecillas, A.; Ferrer, J. (2018). Real-time optimization of the key filtration parameters in an AnMBR: Urban wastewater mono-digestion vs. co-digestion with domestic food waste. *Waste Management*. 80:299-309. <https://doi.org/10.1016/j.wasman.2018.09.031>



The final publication is available at

<http://doi.org/10.1016/j.wasman.2018.09.031>

Copyright Elsevier

Additional Information

Highlights

- Average costs of €0.047 (UWW) and €0.067 per m³ (UWW and FW) were obtained
- Energy costs accounted for 59.6% and 69.0% of the total costs respectively
- Average reversible fouling removal downtimes were 0.4% and 1.6% respectively
- Control strategy efficiently minimized filtration costs for both substrates

1 **Real-time optimization of the key filtration parameters in an AnMBR: urban**
2 **wastewater mono-digestion vs. co-digestion with domestic food waste**

3 A. Robles ^{a,*}, G. Capson-Tojo ^b, M. V. Ruano ^a, A. Seco ^a, J. Ferrer ^c

4
5 ^a CALAGUA – Unidad Mixta UV-UPV, Departament d'Enginyeria Química, ETSE-UV,
6 Universitat de València, Avinguda de la Universitat s/n, 46100, Burjassot, València, Spain.

7 ^b LBE, INRA, Univ. Montpellier, 102 avenue des Etangs, 11100, Narbonne, France

8 ^c CALAGUA – Unidad Mixta UV-UPV, Institut Universitari d'Investigació d'Enginyeria de
9 l'Aigua i Medi Ambient – IIAMA, Universitat Politècnica de València, Camí de Vera s/n,
10 46022, València, Spain

11 * Corresponding author: tel. +34 96 354 30 85, e-mail: *angel.robles@uv.es*

12
13 **Abstract**

14 This study describes a model-based method for real-time optimization of the key filtration
15 parameters in a submerged anaerobic membrane bioreactor (AnMBR) treating urban
16 wastewater (UWW) and UWW mixed with domestic food waste (FW). The method consists
17 of an initial screening to find out adequate filtration conditions and a real-time optimizer
18 applied to a periodically calibrated filtration model for minimizing the operating costs. The
19 initial screening consists of two statistical analyses: (1) Morris screening method to identify
20 the key filtration parameters; (2) Monte Carlo method to establish suitable initial control
21 inputs values. The operating filtration cost after implementing the control methodology was
22 €0.047 per m³ (59.6% corresponding to energy costs) when treating UWW and €0.067 per m³
23 when adding FW due to higher fouling rates. However, FW increased the biogas
24 productivities, reducing the total costs to €0.035 per m³. Average downtimes for reversible

25 fouling removal of 0.4% and 1.6% were obtained, respectively. The results confirm the
26 capability of the proposed control system for optimizing the AnMBR performance when
27 treating both substrates.

28

29 **Keywords**

30 Anaerobic membrane bioreactor (AnMBR); process control; food waste; fouling; modelling;
31 urban wastewater

32

33 **1. Introduction**

34 Submerged anaerobic membrane bioreactors (AnMBRs) are amongst the most promising
35 technologies for treatment of urban wastewater (UWW) (Ben and Semmens, 2002). When
36 compared with traditional processes, such as conventional activated sludge system, AnMBRs
37 offer several advantages (Judd and Judd, 2011; Raskin, 2012): (i) decoupling of hydraulic
38 retention time (HRT) and solids retention time (SRT), (ii) improvement of organic matter
39 removal efficiency, (iii) reduction of the environmental footprint of the treatment process, (iv)
40 production of a solids-free purified effluent, (v) smaller amounts of sludge produced due to
41 the low biomass yield of anaerobic microorganisms, (vi) lower energy demands (no aeration
42 needed), and (vii) energy recovery by biogas production. In addition, the co-digestion in
43 AnMBRs of UWW with domestic food waste (FW) is a very interesting option which may
44 serve to enhance the biogas productivities (*i.e.* by increasing the organic loading rate and the
45 influent COD/SO₄²⁻ ratio), thus improving the general economics of the treatment process
46 (Becker et al., 2017). Moreover, this approach creates an opportunity for recycling energy and
47 nutrients from both wastes (Kibler et al., 2018). This strategy also allows the valorization of
48 domestic FW, whose anaerobic mono-digestion is known to be associated with several
49 complications, such as accumulation of NH₃ and volatile fatty acids (VFAs) (Capson-Tojo et

50 al., 2017, 2016).

51 However, a key issue exists that affects the economics of membrane filtration processes and
52 therefore its industrial applicability: membrane fouling (Deng et al., 2016; Sheets et al.,
53 2015). Fouling reduces the permeability of the membrane, which leads to an increase in the
54 operating and maintenance costs, jeopardizing the global performance (Judd and Judd, 2011).
55 Moreover, previous studies have suggested that fouling issues tend to get worse if adding FW
56 to the UWW (Pretel et al., 2016). Thus, if AnMBRs are to be a competitive alternative for
57 UWW treatment from an economical point of view, minimizing the impact of membrane
58 fouling is of critical importance. Therefore, one of the main challenges of this technology is to
59 optimize the treatment performance (keeping high treatment flow rates) and the energy
60 consumption (small physical cleaning intensities and periods) whilst minimizing the fouling
61 effect. Particularly, avoiding irreversible fouling, which must be removed chemically and
62 eventually determines the lifespan of the membranes, is of critical importance (Drews et al.,
63 2009; Judd and Judd, 2011). Moreover, as the physical cleaning of the membranes can
64 account for more than 75 % of the energetic consumption in AnMBRs (Verrecht et al., 2010),
65 this step must also be optimized, reducing as much as possible its frequency.

66 In this respect, the development of advanced control systems is crucial for a successful
67 optimization of the process performance in AnMBRs (Jimenez et al., 2015; Nguyen et al.,
68 2015). Different studies have assessed theoretically (and sometimes validated experimentally)
69 the energy and economical savings resulting from the implementation of different types of
70 advanced control systems in aerobic membrane reactors (MBRs) (Drews et al., 2007;
71 Huyskens et al., 2011). Mannina and Cosenza (2013) applied Monte Carlo simulations to
72 compare the energy requirements, the effluent quality and the economic costs of five different
73 scenarios based on an MBR model. Also, an ad-hoc platform constructed over the
74 COST/Benchmark Simulation Model No. 1 (BSM1) (Coop, 2002) was applied to evaluate

75 different control strategies in MBRs, using the energy requirements to assess the
76 performances (Maere et al., 2011). Gabarron et al. (2014) compared different optimization
77 strategies applied to MBRs, reducing significantly the energy needs and the membrane
78 fouling. Moreover, Ferrero et al. (2011a, 2011b, 2011c) reduced significant the energy
79 requirements due to membrane scouring (up to 21%) by applying a knowledge-based control
80 system based on a supervisory controller. Focusing on model-based control, Drews et al.
81 (2009, 2007) created a control system based on a mathematical model that successfully
82 improved the filtration efficiency. In addition, Busch et al. (2007) developed a run-to-run
83 control system to optimize the filtration performance by adjusting the filtration variables after
84 each filtration cycle. Recently, computational fluid dynamics simulations have also been
85 applied to optimize membrane scouring and the hydrodynamics in airlift external circulation
86 MBRs (Yang et al., 2017, 2016). These studies allowed a significant reduction of reversible
87 fouling due to cake formation, thus maximizing the MBR performance.

88 However, so far few control strategies have been developed and validated to optimize the
89 performance of AnMBRs for the treatment of UWW (Robles et al., 2013a). In Robles et al.
90 (2013a), an upper layer fuzzy-logic controller efficiently kept low fouling rates, improving the
91 process performance. In addition, a model-based optimization method has also been applied
92 to improve the performance of AnMBRs treating UWW (Robles et al., 2014a). This method
93 was effectively used for optimization of an advanced control system (consisting of an upper-
94 layer fuzzy-logic controller), obtaining energy savings of up to 25 %. Nevertheless, to
95 improve the economic viability of these systems, it is necessary to develop new control
96 strategies that allow the filtration system to work under optimal conditions. These new
97 strategies should be easy to handle and computational-cost effective to facilitate plant
98 engineers to optimize the process performance.

99 Among the different options that exist, the use of model-based control systems is of interest,

100 not only to control the process performance, but also to predict it, allowing eventually its
101 optimization from an energetic and/or economical approach (Batstone et al., 2015; Gernaey et
102 al., 2004; Martin and Vanrolleghem, 2014). Nonetheless, the predictions based on models are
103 never totally free of uncertainty because models are always a conceptual representation of
104 reality and are based on assumptions. Moreover, models need to be calibrated, a process that
105 can be arduous. In this context, sensitivity analysis is a powerful tool that can be used for two
106 main purposes: (i) quantifying the effects of the inputs on the outputs of the model and (ii)
107 identifying the most relevant factors and those that can be disregarded, thus simplifying the
108 calibration process (Pianosi et al., 2016).

109 Therefore, the objective of this study was to develop a model-based control strategy for real-
110 time optimization of the performance of AnMBRs fed with UWW and a mixture of UWW
111 and FW. This strategy aimed at optimizing the operating mode of the filtration process in an
112 AnMBR system by dynamic simulations using a previously validated filtration model..
113 Specifically, the new model-based control strategy consists of an initial screening to find out
114 the adequate filtration conditions and a real-time optimizer of the filtration operation mode.
115 As for the initial screening, two sequential statistical methods were applied only once as a
116 prior step: (i) a sensitivity analysis to find an identifiable input subset for the filtration process
117 (Morris screening method) (Morris, 1991) using the trajectory-based random sampling
118 technique, and (ii) a Monte Carlo procedure to find adequate initial conditions. This initial
119 screening was based on an approach previously used for optimizing the input parameters of an
120 advanced control system for filtration in AnMBRs (Robles et al., 2014a). Regarding the real-
121 time optimizer, an optimization algorithm applied to a filtration model is run to obtain the
122 optimum values of the identifiable subset for the filtration process that minimize the operating
123 costs of the system. This new-model-based controller is more straight-forward when
124 compared to the previous control strategy (Robles et al, 2014b) based on coupling model-

125 based control systems with fuzzy-logic advanced supervisory control, since only a model
126 must be calibrated.

127

128 **2. Materials and methods**

129 To accomplish the besought goal the first approach of the process, which is carried out only
130 once as a prior step, consisted of: (i) a sensitivity analysis that considers the different
131 parameters that are likely to be optimized in a previously chosen model (Robles et al., 2013c,
132 2013d), thus selecting highly-influential parameters conforming the identifiable input subset
133 to be optimized and (ii) the selection of adequate initial conditions (those leading to local
134 minimal operational costs) of the identifiable input subset was performed via the Monte Carlo
135 method. Knowing these values, the real-time optimization of the highly-influential operational
136 parameters was carried out. With this purpose, an optimization algorithm was defined. This
137 real-time optimizer stablished, at every control time (CT), the set points for the operational
138 parameters leading to the lowest costs of the filtration process. Finally, the reduction of the
139 total costs of the filtration process after the implementation of the control system was assessed
140 (with and without FW in the substrate).

141 *2.1. Description of the AnMBR plant*

142 The data used in this study to calibrate and validate the filtration model was obtained from an
143 AnMBR that mainly consisted of an anaerobic reactor with a working volume of 0.9 m³
144 connected to two membrane tanks. Each membrane tank had a working volume of 0.6 m³ and
145 included one ultrafiltration hollow-fiber membrane commercial system (PURON[®], Koch
146 Membrane Systems, 0.03 μm pore size, 31 m² total filtering area and outside-in filtration).
147 The plant was fully automated and monitored online in real-time. In addition, the anaerobic
148 sludge was sampled once a day to assess the filtration performance. The concentration of
149 mixed liquor total solids (MLTS) was determined according to the Standard Methods (APHA,

150 2005). A more precise description of the plant and its instrumentation (as well as the
151 corresponding flow diagrams) can be found elsewhere (Robles et al., 2015, 2013b).

152 *2.1.1. Lower-layer controllers*

153 The lower-layer controllers implemented in the system that interact with the proposed
154 optimization method are: (i) three proportional-integral-derivative (PID) controllers that
155 adjust the rotating speed of the sludge recycling pump, the permeate pump and the biogas
156 recycling blower used for membrane scouring by gas sparging, in order to keep the desired
157 flow-rate set-points; and (ii) one on–off controller that regulates the membrane operating
158 stage by changing the position of the respective on–off valves and the flux direction of the
159 permeate pump. A more precise description of the plant control system can be found
160 elsewhere (Robles et al., 2015).

161 *2.2. Characteristics of the substrates*

162 As aforementioned, the proposed model-based optimization strategy was validated for an
163 AnMBR treating UWW and a mixture of UWW and FW. To this aim, a filtration model was
164 calibrated and validated using data from an AnMBR system that treated UWW and a mixture
165 of UWW and FW. The UWW was the effluent from the pre-treatment step of the Carraixet
166 WWTP (Valencia, Spain) and the FW was collected from canteens in the university (Moñino
167 et al., 2016). The UWW was characterized by a low COD/SO₄-S ratio and the mixture of
168 UWW and FW was set to different penetration factors (PF, defined as the percentage of the
169 population having a kitchen disposer). The COD/SO₄-S ratio of the UWW was around 6.6 kg
170 COD·kg⁻¹ SO₄-S while the COD/SO₄-S ratio of the UWW was around 9.6 kg COD·kg⁻¹ SO₄-
171 S. The FW was grinded by an experimental set-up simulating a household grinding system.
172 This set-up consisted on a grinded InSinkErator, model Evolution 100. Afterwards, the FW
173 was pre-filtered using a mesh of 0.5 mm, similar to the one used for the UWW. Further details
174 can be found elsewhere (Moñino et al., 2017).

175 *2.3. Description of the filtration model*

176 The filtration model used in this study is a semi-empirical model based on a classical
177 resistance-in-series model (Robles et al., 2013c). This model is able to represent the dynamic
178 evolution of the transmembrane pressure (TMP) by equations 1 and 2.

$$TMP(t) = J_{net} \cdot \mu_p \cdot R_T \quad (\text{Eq. 1})$$

179 Where, TMP (t) is the TMP at time t, μ_p is the dynamic viscosity of the permeate and R_T is
180 the total filtration resistance.

$$R_T = R_M + R_C + R_I = R_M + \omega_C \cdot \alpha_C + \omega_I \cdot \alpha_I \quad (\text{Eq. 2})$$

181 Where, R_M is the resistance intrinsic to the membrane, R_C is the resistance of the cake that is
182 formed on the surface of the membrane due to solid deposition, R_I is the added resistance due
183 to irreversible membrane fouling, ω_C is the mass of solids deposited on the membrane per
184 membrane area, α_C is the average specific resistance of the cake created, ω_I is the mass of
185 irreversible fouling normalized per membrane area and α_I is the average specific resistance of
186 the irreversible fouling.

187 The dynamics of ω_C and ω_I were modelled using a black-box approach. With this purpose,
188 three different components were defined: X_{TS} (MLTS), X_{mC} (cake dry mass in the membrane
189 surface), and X_{mI} (irreversible fouling dry mass on the membrane surface). In addition, four
190 kinetic physical processes were included in the model: (i) cake layer formation during
191 filtration, (ii) cake layer removal by biogas sparging for membrane scouring, (iii) cake layer
192 removal by back-flushing and (iv) irreversible fouling formation. A more precise description
193 of the structure of the filtration model can be found elsewhere (Robles et al., 2014a).

194 The selected filtration model was calibrated and validated using experimental data from the
195 above-introduced AnMBR plant when treating UWW and a mixture of UWW and FW.

196 *2.4. Model-based optimization*

197 As aforementioned, the first stage of the model-based control strategy is the selection of the
198 operational parameters associated with the filtration process that are likely to be optimized
199 dynamically. These variables are the biogas recycling flow-rate for membrane cleaning
200 (BRF), the sludge recycling flow-rate into the membrane tanks (SRF), the duration of the
201 filtration, relaxation and back-flushing stages (t_F , t_R and t_{BF} respectively) and the initiation
202 frequency and transmembrane flow of the back-flushing stage (f_{BF} , J_{BF}). It must be
203 commented that the transmembrane flow during filtration (J_F) has not been considered for the
204 optimization. The reason is that this value will be fixed by the influent flow-rate to the
205 system.

206 Considering these selected variables, the operating mode of the membranes can be
207 represented by Figure 1A. As this figure shows, an alternation is established between the
208 relaxation and the back-flushing stages. More precisely, if the number of filtration cycles (f) is
209 lower than f_{BF} , the system will alternate between filtration and relaxation cycles. However, if
210 f_{BF} is equal or overpasses f , the corresponding relaxation stage will be substituted by a back-
211 flushing stage. Figure 1B shows a schematic representation of the model-based control
212 strategy applied in this study, which is divided in an initial screening and a real-time
213 optimizer of the filtration operation mode. The initial screening is based on a procedure
214 described in Robles et al., (2014a) for screening the input parameters of an advanced control
215 system for filtration in AnMBRs and the real-time optimizer uses the previously introduced
216 filtration model for calculations (Robles et al., 2013c). First of all, the Morris screening
217 method (Morris, 1991) was used to perform a global sensitivity analysis (GSA) of the selected
218 filtration model (step a) to identify the operational parameters with high influence on the cost
219 of the filtration process (step b). Once these parameters were identified, the Monte Carlo
220 procedure (see for instance Saltelli et al. (2000) was applied to determine the optimal initial
221 values of the evaluated parameters (step c). These values are used to update the initial set-

222 points of the operational parameters (step d), which are transferred to the process (step e).
 223 After the transmission of the initial set-points, every CT the optimization algorithm is started.
 224 In this work CT has been set to 1 hour. This real-time optimizer, calculates the new optimal
 225 set-points for the highly-influential operational parameters at each CT (step f), running the
 226 periodically calibrated filtration model, and transmits them (step g) to update again the set-
 227 points of the process (steps d and e). To this aim, a cost objective function was used.

228 2.4.1. Description of the costs objective function

229 To determine the costs related to energy consumption, the energy requirement of each process
 230 was calculated and multiplied by the cost of energy (E_{COST} ; € per kWh). In this study E_{COST}
 231 was set to €0.138 per kWh, which corresponded to average electricity prices in Spain.

232 The energy requirements of the blower (W_{BRF}) (adiabatic compression), sludge recycling
 233 pump (W_{SRF}) and permeate pump for filtration ($W_{filtration}$) or back-flushing ($W_{back-flusing}$) were
 234 calculated as shown in Robles et al. (2014a).

235 The total energetic costs were lumped in a single variable (C_W), which was calculated as the
 236 sum of C_{BRF} , C_{SRF} and C_{STAGE} , as shown in Equation 3:

$$C_W = C_{BRF} + C_{SRF} + C_{STAGE} = W_{BRF} \cdot E_{COST} + W_{SRF} \cdot E_{COST} + W_{STAGE} \cdot E_{COST} \quad (\text{Eq. 3})$$

237 Where, C_W is the total energetic cost, C_{BRF} is the operating cost of membrane scouring by
 238 biogas sparging, C_{SRF} is the operating cost of pumping the sludge, C_{STAGE} is the operating cost
 239 of pumping permeate during the respective operating stage (*i.e.* filtration or back-flushing).

240 Finally, in order to determine the combination of operational set-points that lead to the
 241 minimal value of the total operating costs (C_{TOTAL} ; € per m^3), Equation 4 was applied.

$$C_{TOTAL} = C_W + C_{REAGENTS} + C_{LIFESPAN} \quad (\text{Eq. 4})$$

242 Where, C_W is the total energetic cost, $C_{REAGENTS}$ is the proportional cost of reagents needed to
 243 clean the irreversible fouling produced during filtration and $C_{LIFESPAN}$ is the cost of membrane

244 replacement due to irreversible fouling. C_{REAGENTS} and C_{LIFESPAN} were calculated as shown in
245 Robles et al. (2014a).

246 *2.4.2. Global sensitivity analysis: Morris screening method*

247 In this study the Morris screening method (Morris, 1991) has been applied to perform the
248 GSA. This method is a one-factor-at-a-time process based on the generation of representative
249 matrices of the combinations of values of the parameters to evaluate through a random
250 sampling. In this study, the trajectory-based sampling strategy proposed in Ruano et al. (2012)
251 was applied. From the matrices, it determines the distribution of scaled elementary effects
252 (SEE_i) of each input factor on the model output. Finally, the SEE_i distribution (F_i) for each
253 input factor is analyzed to determine the relative importance of the input factors and obtain a
254 good approximation of a GSA.

255 The selected statistical parameters to evaluate these distributions were: the standard deviation
256 (σ) and the absolute mean (μ^*) (see for instance Saltelli et al. (2000) and Campolongo et al.
257 (2007)).

258 In order to elucidate which operational parameters are the most influential on the total
259 filtration cost, the output variable for the GSA in this study was C_{TOTAL} (Eq. 4).

260 A more precise description of the GSA applied in this study can be found elsewhere (Robles
261 et al., 2014b).

262 *2.4.3. Initial values of the operational parameters: Monte Carlo method*

263 The Monte Carlo method was used for the selection of initial values of the operational
264 parameters close to the minimum (locally) of the function to minimize. This has two main
265 benefits: (i) it improves the results of the dynamical optimization given by the controller and
266 (ii) it gives optimal values of the non-influential parameters, further improving the
267 minimization of C_{TOTAL} . Therefore, the Monte Carlo method was applied as a previous step
268 before the dynamic optimization. The Monte Carlo method consisting on trajectory-based

269 random sampling was used in this study. Hence, the combination of the operational
270 parameters giving the minimum operating cost (Eq. 4) was selected as the initial values of the
271 real-time optimizer.

272 *2.4.4. Simulation strategy and model calibration*

273 MATLAB[®] was used to simulate the filtration process using the previously-introduced model.
274 The Runge-Kutta method (ode45 function in MATLAB[®]) was used as integration method for
275 solving the differential equations in the model. The model was calibrated using experimental
276 results from operation with both substrates.

277 *2.4.5. Simulations for real-time dynamic optimization of the filtration process*

278 The dynamic optimization of the filtration process was carried out using the costs equation
279 (Eq. 4) as objective function. The optimization algorithm was applied by using the trust
280 region approach (Coleman and Li, 1996), based on the Newton method (LSQNONLIN
281 function in MATLAB[®]) and the Runge-Kutta method (ode45 function in MATLAB[®]).

282 *2.4.6. Implementation of the Morris and Monte Carlo methods*

283 In order to obtain results that could be extrapolated to different situations, MLTS
284 concentrations in the entrance of the membrane tanks was ranged from 10 to 20 g·l⁻¹ during
285 simulation. In addition, to take into account the typical fluctuations of the flow rate entering a
286 WWTP, the net transmembrane flow (J_{net}) was also varied. For each concentrations of MLTS,
287 J_{net} was modified from 4 to 12 LMH ($l \cdot h^{-1} \cdot m^{-2}$), following the influent pattern from the model
288 BSM1 (Jeppsson et al., 2006).

289 The average values of the operational parameters evaluated in this study are shown in Table 1.
290 In addition, the uncertainty considered for the sensitivity analysis (minimum and maximum
291 values) is also presented. The range of values for the set-points of these parameters was
292 established according to a uniform distribution. Finally, the results of the Monte Carlo
293 procedure (which will be discussed afterwards) are also shown in Table 1.

294 2.4.7. Optimization algorithm

295 Using both substrates, the performance of the controller (based on the optimization algorithm)
296 was evaluated by simulation using the filtration model described above. The simulation
297 accounted for 24 h of continuous operation and was carried out at four different MLTS
298 concentrations entering the membrane tanks for both feeding strategies (*i.e.* UWW and
299 mixture of UWW and FW): 11, 13, 15 and 17 g·l⁻¹.

300 To simulate the important variations of the influent flow rate that occur in WWTPs, the
301 dynamic of BSM1 influent (Jeppsson et al., 2006) was used in this simulation study,
302 commonly accepted for evaluation of control algorithms in WWTPs (Maere et al., 2011,
303 Rojas et al., 2012; Martin and Vanrolleghem, 2014; Foscoliano et al., 2016). Thus, during the
304 simulations J_{net} varied according to the dynamic of BSM1 influent (see e-supplementary
305 data).

306 As aforementioned, the CT was set to 1 hour. The computational cost for optimizing
307 dynamically the process was between 1 to 3 minutes (using a PC Intel® CORE™ i5 with 8
308 GBytes of RAM).

309 3. Results and discussion

310 3.1. Overall performance of the AnMBR plant

311 The AnMBR plant, treating either UWW or UWW mixed with domestic FW, was operated
312 for a long period within a wide range of operating conditions regarding both biological and
313 filtration processes (Robles et al., 2013c; Giménez et al., 2011, Pretel et al., 2016; Moñino et
314 al., 2017).

315 Generally, COD removal efficiencies above 90 % were obtained, while effluent COD
316 concentration ranged between 23 and 54 mg·l⁻¹. The VFA in the reactor showed an average
317 value of 30 mg HAc·l⁻¹, which is significantly lower than the common concentrations found
318 in other anaerobic digestion processes. Methane production increased significantly when

319 operating at high SRT and/or when adding domestic FW to the substrate. For instance, 30 and
320 $56 \text{ l}_{\text{CH}_4} \cdot \text{m}^{-3}$ were obtained when treating UWW at SRTs of 40 and 70, respectively. These
321 values are not so high due to the significant sulfate concentration in the influent, thus, a
322 considerable amount of influent COD was consumed by sulfate reducing bacteria.

323 Nonetheless, methane production increased up to $119 \text{ l}_{\text{CH}_4} \cdot \text{m}^{-3}$ when treating a mixture of
324 UWW and FW with a penetration factor of 80 % and 70 days of SRT.

325 As for sludge production, lower amounts of wasted sludge were produced when operating at
326 high SRT and/or feeding UWW mixed with domestic FW. The obtained $0.37 \text{ kg TSS} \cdot \text{kg}^{-1}$
327 $\text{COD}_{\text{REMOVED}}$ of wasted sludge at a SRT of 70 days for UWW treatment was reduced up to
328 $0.21 \text{ kg TSS} \cdot \text{kg}^{-1} \text{COD}_{\text{REMOVED}}$ when treating a mixture of UWW and FW with a penetration
329 factor of 80 % at the same SRT.

330 Concerning the filtration process, the fouling rates were mainly governed by the MLTS and
331 the specific demands of gas per square meter of membrane (SGD_m) levels. However other
332 factors should also be considered, such as the characteristics of the sludge (i.e. SMP, EPS,
333 biomass). Mostly, for similar SGD_m values, as MLTS levels surged the fouling rates
334 increased. It is important to note that low values of the fouling rates were observed (below 10
335 $\text{mbar} \cdot \text{min}^{-1}$ for negligible levels of irreversible fouling) when treating UWW at an SGD_m of
336 $0.23 \text{ Nm}^3 \cdot \text{h}^{-1} \cdot \text{m}^{-2}$ (equivalent to a BRF of $7.1 \text{ m}^3 \cdot \text{h}^{-1}$) and MLTS levels below $25 \text{ g} \cdot \text{l}^{-1}$ (ranging
337 from 8 to $32 \text{ g} \cdot \text{l}^{-1}$). Above $25 \text{ g} \cdot \text{l}^{-1}$ of MLTS, the membrane fouling surged sharply (around
338 $100 \text{ mbar} \cdot \text{min}^{-1}$) for similar SGD_m values. Nonetheless, these fouling rates were reduced
339 when the SGD_m levels raised up to non-prohibitive levels (from 0.23 to $0.5 \text{ Nm}^3 \cdot \text{h}^{-1} \cdot \text{m}^{-2}$,
340 equivalent to BRFs of 7.1-15.5 $\text{m}^3 \cdot \text{h}^{-1}$), taking into account that the effect of the gas sparging
341 intensity was reduced as the irreversible fouling increased. The results obtained during long-
342 term operation of membranes reinforced the need for optimizing the membrane scouring at
343 each operating condition.

344 When treating UWW and domestic FW, fouling rates surged as the penetration factor in the
345 mixture increased. For instance, a permeability loss of $0.14 \text{ LMH bar}^{-1} \cdot \text{m}^{-3}$ was obtained
346 when treating UWW at MLTS of $17 \text{ g} \cdot \text{l}^{-1}$. In contrast, permeability losses of up to 0.38 LMH
347 $\text{bar}^{-1} \cdot \text{m}^{-3}$ were obtained when feeding a mixture of UWW and FW with a penetration factor of
348 80 %.

349 *3.2. Calibration of the model*

350 Before the application of the model, it was previously calibrated and validated based on the
351 data obtained in the AnMBR plant treating both UWW and a mixture of UWW and FW. More
352 precisely, the model was validated for different concentrations of MLTS entering the
353 membrane tanks ($10\text{-}30 \text{ g} \cdot \text{l}^{-1}$), different J_{net} ($4\text{-}6 \text{ LMH}$) and different SDG_m ($0.1\text{-}0.5 \text{ m}^3 \cdot \text{h}^{-1} \cdot \text{m}^{-2}$,
354 equivalent to BRFs of $3.1\text{-}15.5 \text{ m}^3 \cdot \text{h}^{-1}$). The model was able to predict precisely the
355 behavior of the membrane during the studied operational conditions (R of 0.989). It is
356 important to note that a recalibration of the filtration model must be done periodically to take
357 into account possible fluctuations such as influent load dynamics (*i.e.* heterogeneity of FW
358 and UWW).

359 *3.3. Sensitivity analysis*

360 *3.3.1. Treating urban wastewater*

361 The rankings for the operational parameters according to the sensitivity measurements
362 obtained (μ^* and σ) are presented in Table 2. Only the results for the optimized number of
363 evaluated trajectories (r_{opt}) are shown.

364 Hierarchical clustering analysis (HCA; R software version 3.2.5.) of the μ^* presented in Table
365 2 and the ones obtained during r_{opt} determination resulted in three differentiated clusters
366 formed according to the influence of the studied parameters on the model output (see e-
367 supplementary data): (i) BRF, with a much higher value of μ^* when compared with the other
368 parameters, indicating its great importance for the process costs; (ii) f_{BF} , t_{BF} , t_{F} and SRF, with

369 values of μ^* that indicate a significant relative influence on the process costs; and (iii) t_R and
370 J_{BF} , with a low relative importance. According to these results, 5 parameters were identified
371 as highly influential on the process costs: (i) BRF ($\mu^* = 1.253$ and $\sigma = 1.856$); (ii) f_{BF} ($\mu^* =$
372 0.770 and $\sigma = 2.220$); (iii) t_F ($\mu^* = 0.724$ and $\sigma = 1.921$); (iv) t_{BF} ($\mu^* = 0.574$ and $\sigma = 1.210$);
373 and (v) SRF ($\mu^* = 0.464$ and $\sigma = 1.584$). To allow a visual identification of these parameters, a
374 graphical representation of the results of the sensitivity parameters (μ^* and σ) at r_{opt} can be
375 found in the Electronic Annex. Both the clustering and the graphical results suggest a high
376 influence of BRF, SRF, t_F , t_{BF} and f_{BF} on the cost of the process. Therefore, in this study they
377 have been optimized dynamically as a function of the operational conditions. On the other
378 hand, as t_R and J_{BF} present low values of μ^* and σ , it can be considered that their influence on
379 the total costs is low. Thus, their set-points were considered to be constant, keeping the initial
380 values given by the Monte Carlo method. In addition, the GSA results allow evaluating the
381 mathematical relationship between each parameter and the total costs. Due to their relative
382 high values of both μ^* and σ , the effects of BRF, SRF, t_F , t_{BF} and f_{BF} can be classified as non-
383 linear.

384 The huge influence of BRF was related to the high energy consumption of this process. Thus,
385 while an adequate value of BRF allows minimizing the solid cake formation, the irreversible
386 fouling rates, and the costs associated with biogas recirculation, too high values increase
387 greatly the total costs of the filtration process. Concerning SRF, this parameter affects, not
388 only the costs associated with sludge pumping, but also $MLTS_{MT}$ at a given J_{net} . It is
389 important to consider that changes of the $MLTS_{MT}$ modify also the BRF requirements. In
390 addition, t_F affects the amount of solids that are deposited onto the surface of the membranes.
391 t_F also influences the net water treatment flow, thus determining the normalized profitability
392 of the process (expressed in € per m^3). Finally, t_{BF} and f_{BF} modify the extent of permeability
393 recovery of the membranes. This is related to a partial or total removal of the solid cake.

394 However, it must also be considered that high values of t_{BF} and f_{BF} decrease J_{net} and increase
395 the non-filtration period of the AnMBR.

396 *3.3.2. Treating urban wastewater and food waste*

397 The values of the sensitivity measurements (μ^* and σ) obtained for the optimized number of
398 evaluated trajectories ($r_{opt} = 40$) when using UWW and FW as substrates are presented in
399 Table 2. The corresponding HCA (see e-supplementary data) resulted in very similar clusters
400 when compared to the process treating only UWW. In this case, 5 main clusters were
401 obtained: (i) BRF, again with a much higher value of μ^* when compared with the other
402 parameters; (ii) f_{BF} , with higher relative values when compared to treatment of only UWW;
403 (iii) t_{BF} and t_F , also with values of μ^* that indicate a significant relative influence; (iv) SRF
404 and t_R , with a low relative influence; and (v) J_{BF} , with a very low relative importance. The
405 similar responses of the systems fed with UWW and the mixture of UWW and FW confirm
406 the applicability of the optimization methodology evaluated in this study to both substrates. In
407 order to allow an un-biased comparison of the performances of the controller using both
408 substrates, the same five operational parameters were identified as influential: BRF, f_{BF} , t_{BF} , t_F
409 and SRF. However, it must be considered that the clustering results suggest that in this case
410 SRF could also be kept constant, reducing even more the computational costs. As for the case
411 using UWW as substrate, a graphical representation of the obtained sensitivity rankings
412 treating the UWW and FW mixture is presented in the Electronic Annex.

413 *3.4. Initial parameter estimation via the Monte Carlo method*

414 As aforementioned, the Monte Carlo method was used to estimate the initial values of the
415 different operational parameters object of study when applying both feeding strategies (*i.e.*
416 UWW and mixture of UWW and FW). The total filtration cost varied greatly, with values
417 ranging between €0.04 per m^3 and €0.40 per m^3 . Therefore, it can be concluded that the total
418 costs can be effectively minimized by selecting the proper set-points of the selected

419 operational parameters.

420 The obtained results, which correspond to the combination leading to minimum local costs,
421 are presented in Table 1 (column Monte Carlo Results). However, it is important to highlight
422 that the Monte Carlo method cannot give an optimal combination of the operational
423 parameters. This occurs because of the discrete variation of the values of the evaluated
424 parameters chosen to carry out the simulations. Nevertheless, as the used sampling procedure
425 aims at covering all the domain of variation of the parameters, the cost is locally minimized.
426 Starting from the initial combination given by the Monte Carlo method, the selected
427 parameters were optimized dynamically throughout the operational period.

428 *3.5. Performance of the real-time optimizer*

429 *3.5.1. Treating urban wastewater*

430 Figure 2 shows the values of BRF, SRF, t_F and t_{BF} optimized by the controller during the
431 simulations performed with a MLTS concentration entering the membrane tank of $17 \text{ g}\cdot\text{l}^{-1}$ and
432 the transmembrane fluxes shown in the e-supplementary data. This condition is presented
433 because it is the worst-case scenario, meaning that in reality the performance should be
434 improved, with less fouling and lower filtration costs when reducing MLTS_{MT} .

435 As shown in Figure 2A, the value of BRF followed a very similar pattern when compared to
436 J_{net} . This occurred because the controller established higher values of BRF in the periods
437 when the treatment flow rate was the highest (10-13 hours). During those flow peaks, the
438 velocity of solid deposition on the surface of the membrane was much higher than at regular
439 operation and therefore the controller had to increase considerably BRF to keep the TMP at
440 appropriate values. In addition, Figure 2A also shows that the value of BRF was reduced
441 when the treatment flow decreased, reaching even the minimum BRF value allowed in the
442 AnMBR plant ($4 \text{ m}^3\cdot\text{h}^{-1}$). These conditions corresponded to the minimal membrane fouling
443 propensity, but were also associated with low agitation of the sludge in the membrane tanks,

444 leading to a reduction in the efficiency of the process of physical cleaning by biogas sparging.
445 A correlation matrix including the optimized parameters, $MLTS_{MT}$, J_{net} , TMP, the energy
446 requirements and the filtration costs with UWW as substrate (see e-supplementary data; R
447 software version 3.2.5.) verified the positive correlation observed between J_{net} , TMP and
448 BRF.

449 Regarding SRF, Figure 2A shows a similar behavior to that observed for BRF. The controller
450 increased SRF at higher J_{net} to keep $MLTS_{MT}$ at adequate levels. Again, the correlation matrix
451 verified the correlation existing between BRF and SRF.

452 Concerning t_F and t_{BF} , it can be observed in Figure 2B that in this case these variables did not
453 follow a pattern similar to that of J_{net} . However, a variation of these parameters occurred
454 through the operational period studied. Interestingly, the periods when t_F and t_{BF} varied the
455 most were those when BRF and SRF showed their lowest values (*i.e.* 5-9 h and 19-24 h). This
456 indicates that, when the controller could not further optimize BRF and SRF, it modified the
457 parameters with lower influence (*i.e.* t_F and t_{BF}) to further minimize the total filtration costs.
458 No linear correlations were observed between t_F and t_{BF} and any other studied
459 parameter/variable (see e-supplementary data). The last parameter to be discussed (f_{BF})
460 remained relatively constant, around 1 BF every 10 F cycles (see Figure 3).

461 Figure 3 represents the evolution of the TMP and the sequence of operational stages (F, R and
462 BF) performed during the simulation at $17 \text{ g}\cdot\text{l}^{-1}$ $MLTS$ entering the membrane tanks.

463 As it can be observed, the operational mode varied according to the duration of the stages (t_F
464 and t_{BF}). In addition, by increasing SRF and BRF (Figure 2A) during the periods most prone
465 to fouling (hours 10-12), the real-time optimizer was able to keep the TMP under the
466 maximum limits established by the provider (*i.e.* 0.6 bars).

467 3.5.2. Treating urban wastewater and food waste

468 Figure 4 shows the values of BRF, SRF, t_F and t_{BF} optimized by the model-based controller

469 when treated UWW and FW. As for the operation with UWW as substrate (Figure 2A), the
470 values of BRF and SRF varied according to the variations in J_{net} (see e-supplementary data).
471 As previously, the controller established higher values of both parameters at the points of
472 highest J_{net} (10-13 hours). This period corresponded to the greatest rates of solids deposition
473 onto the membranes. Therefore, the controller increased BRF to reduce the fouling rate and
474 increased also SRF to minimize $MLTS_{MT}$.

475 In addition, it can be observed in Figure 4B that the values of t_F are lower than those obtained
476 with UWW as substrate (Figure 2B). Interestingly, the opposite occurred for t_{BF} , whose length
477 was higher with the mixture of UWW and FW. This was related to a more intense fouling
478 caused by the FW, which led to longer BF periods to remove the cake layer from the
479 membrane surface. Moreover, f_{BF} increased from 1 BF every 10 F cycles to 1 BF every 4 F
480 cycles (data not shown). Longer t_{BF} and higher f_{BF} with FW led to an increase of the
481 downtime for reversible fouling removal. The average downtime for reversible fouling
482 removal increased from 0.4 % (UWW) to 1.6 % (UWW and FW) of the total operational
483 period. Nevertheless, it must be considered that these are low values which were achieved as a
484 result of the controller action. As example, previous studies have reported minimum values of
485 2.4 % of downtime when treating UWW in an automatically-tuned advanced control system
486 for AnMBRs (Robles et al., 2014a).

487 It must be mentioned that the corresponding correlation matrix (see e-supplementary data)
488 was very similar to that obtained for UWW as substrate, verifying that the controller
489 responded in a similar manner for both substrates. Also, as the evolution of the TMP and the
490 different stages simulated using the substrate mixture were similar to that of UWW treatment
491 (Figure 3), these values are not presented.

492 *3.6. Total energy consumption*

493 Figure 5A shows the evolution of the energy requirements of the filtration process after the

494 implementation of the controller at $17 \text{ g}\cdot\text{l}^{-1}$ MLTS entering the membrane tank with UWW as
495 substrate. As it can be observed, the main contributor to the energy consumption of the system
496 was W_{BRF} , accounting in average for 80 % of the total energy requirements and up to 87 % at
497 the highest J_{net} . In addition, W_{BRF} (thus W_{TOTAL}) shows a similar pattern to that observed for
498 J_{net} . In fact, both variables were strongly correlated (see e-supplementary data). While during
499 the periods of low inflow to the plant (*i.e.* hours 2-9) W_{TOTAL} reached $0.13 \text{ kWh}\cdot\text{m}^{-3}$ (with
500 W_{BRF} accounting for 67 %), this value increased up to $0.34 \text{ kWh}\cdot\text{m}^{-3}$ (with W_{BRF} accounting
501 for 87 %) at high J_{net} (*i.e.* hours 9-12). At this point it must be mentioned that the results
502 shown in this study were obtained with a model calibrated using considerably dirty
503 membranes (*i.e.* the membranes were already strongly irreversibly fouled). Therefore, the
504 energy requirements presented correspond to a very unfavorable scenario and it can be
505 expected that their values will be considerably lower when operating with clean membranes.
506 Nevertheless, the proposed control strategy allowed keeping the W_{BRF} within low values
507 (around $0.18 \text{ kWh}\cdot\text{m}^{-3}$). More precisely, the control system led to savings of around 50 % of
508 the energy required for membrane scouring when compared to non-optimized cyclic operation
509 of the same AnMBR plant ($0.36 \text{ kWh}\cdot\text{m}^{-3}$) (Robles et al., 2013a). By coupling model-based
510 control systems with fuzzy-logic advanced supervisory control, consumptions of $0.15 \text{ kWh}\cdot\text{m}^{-3}$
511 ³ (Robles et al., 2013a) and $0.12 \text{ kWh}\cdot\text{m}^{-3}$ (Robles et al., 2014a) were achieved. The value
512 obtained in this study was slightly higher ($0.18 \text{ kWh}\cdot\text{m}^{-3}$). However, it must be considered
513 that in this case only a model must be calibrated, which can be continuously optimized by
514 retrofitting. In addition, if the model is properly calibrated this control strategy is more
515 straight-forward and the control action is faster when compared to the previous control
516 strategies, which require more computational capacity.

517 When paying attention to the average energy requirements of the AnMBR after the
518 implementation of the control system (Table 3), it can be observed that from the total

519 consumption of $0.20 \text{ kWh}\cdot\text{m}^{-3}$ (operating at $17 \text{ g}\cdot\text{l}^{-1}$ MLTS entering the membrane tanks), 79.7
520 % corresponded to W_{BRF} , $16.9 \text{ kWh}\cdot\text{m}^{-3}$ to W_{SRF} , 9.53 % to $W_{\text{back-flushing}}$ and 4.77 % to
521 $W_{\text{filtration}}$.

522 The results presented in Figure 5 and Table 3 show that the energy required to clean
523 physically the membranes by biogas sparging (W_{BRF}) represents the main consumption of
524 energy in AnMBRs. Thus, there is a clear need to optimize this particular process.

525 Figure 5B and Table 3 also show the energy consumption of the filtration process treating
526 UWW and FW. In this case, the average total requirement was $0.34 \text{ kWh}\cdot\text{m}^{-3}$, with a
527 maximum value of $0.58 \text{ kWh}\cdot\text{m}^{-3}$. The average proportion of W_{BRF} accounted for 88.5 %,
528 indicating the need of optimizing BRF for each specific process.

529 The higher average W_{TOTAL} when adding FW (0.34 vs. $0.20 \text{ kWh}\cdot\text{m}^{-3}$) was related to the
530 aforementioned increase of the fouling rate in the membranes, which implied longer non-
531 filtration periods, thus reducing the net volume of water treated per unit of membrane surface.
532 However, it must be considered that the addition of FW also led to a higher energy recovery
533 due to an increase of the biogas production. With a SRT of 70 days at a temperature of $27 \text{ }^\circ\text{C}$,
534 the volumetric methane production was up to $72 \text{ l}_{\text{CH}_4}\cdot\text{m}^{-3}$ using UWW as substrate (Pretel et
535 al., 2016). When adding FW, this value increased up to $147 \text{ l}_{\text{CH}_4}\cdot\text{m}^{-3}$ which, assuming a
536 percentage of methane recovery of 80 %, was translated into an increase of the energy
537 recovery of $0.20 \text{ kWh}\cdot\text{m}^{-3}$. Taking this value into account, the energy requirements of the
538 filtration process are lowered from $0.34 \text{ kWh}\cdot\text{m}^{-3}$ to $0.14 \text{ kWh}\cdot\text{m}^{-3}$, even when operating with
539 strongly fouled membranes. Thus, the addition of FW led to a global energy saving of 30 %
540 when compared to the treatment of UWW as sole substrate because of the increased
541 volumetric methane production. The energy requirements of the filtration process with the
542 controller operating at 11, 13, 15 and $17 \text{ g}\cdot\text{l}^{-1}$ for both feeding strategies are summarized in
543 the e-supplementary data.

544 3.7. Total costs

545 Figure 6A shows the evolution of the operational and maintenance costs of the filtration
546 system after the implementation of the model-based control strategy treating UWW at $17 \text{ g}\cdot\text{l}^{-1}$
547 MLTS. As it can be observed, C_W represented the main cost of the process, accounting for an
548 average of 60 % of the total cost. This clearly emphasizes the need to optimize the operational
549 conditions to minimize the energy demand of the system. However, in the period of peak J_{net}
550 (hours 9-10) the ensemble of C_{REAGENTS} and C_{LIFESPAN} represented up to 90 % of the total
551 costs. This was related to a more intense irreversible fouling occurring in this period of high-
552 rate filtration, which caused an increase in the amounts of chemicals required to clean the
553 membranes and lowered the membrane lifespan, raising the associated costs.

554 Regarding the average costs, the results operating at $17 \text{ g}\cdot\text{l}^{-1}$ MLTS entering the membranes
555 are presented in Table 4. After the implementation of the control system, C_{TOTAL} was €0.047
556 per m^3 , with C_W , C_{REAGENTS} and C_{LIFESPAN} representing the 59.6, 17.0 and 23.4 %,
557 respectively.

558 These values corroborate that C_W represents the main filtration costs during regular operation.
559 In addition, as it has been already mentioned, the membranes used in this study were strongly
560 fouled, and therefore lower costs are expected in real operation. Thus, the values of these
561 latter costs should be lower in full-scale plants, further reinforcing the great importance of
562 optimizing the energy requirement in AnMBR plant.

563 Figure 6B and Table 4 present the costs corresponding to the co-digestion system (UWW and
564 FW). As shown, the obtained pattern was very similar to that obtained for treatment of UWW.
565 However, in this case the average filtration cost corresponded to €0.067 per m^3 , with C_W
566 accounting for 69 % of this value. The higher value of C_{TOTAL} when adding FW is again
567 related to a higher fouling rate in the co-digestion system, which led to higher costs associated
568 with the mechanical cleaning of the membrane. This is further suggested by the higher C_W

569 values (€0.046 per m³ with FW vs. €0.028 per m³ with only UWW).
570 However, when taking into account the economical profit related to the higher volumetric
571 methane production when adding FW to the UWW, C_{TOTAL} is reduced to €0.035 per m³,
572 meaning that FW addition led a relative economic saving of 26 % of the filtration costs (when
573 compared with the AnMBR system treating only UWW).
574 The average costs of the filtration process with the controller operating at 11, 13, 15 and 17
575 g·l⁻¹ for both feeding strategies are summarized in e-supplementary data.

576

577 **4. Conclusions**

578 The proposed methodology enabled identifying the most influential filtration parameters and
579 selecting proper initial set points for their optimization. The controller allowed a real-time
580 optimization of these set-points, obtaining an energy demand of 0.20 kWh·m⁻³ (79.7% W_{BRF})
581 and a cost of €0.047 per m³ (59.6% C_w) when treating UWW. The addition of FW increased
582 the energy demand and the costs (0.34 kWh·m⁻³ and €0.067 per m³) due to higher fouling
583 intensity, but also led to the production of more biogas. In this respect, further research must
584 be focused on enhancing biological process to surge methane production giving the minimum
585 operating costs, *i.e.* coupling biological with filtration process control. The obtained results
586 confirm the applicability of the proposed control system for optimizing the AnMBR
587 performance when treating both substrates. An automatic recalibration of the filtration model
588 according to the dynamics of the influent characteristics will be necessary to improve the real-
589 time optimizer.

590

591 **Acknowledgements**

592 This research work was possible thanks to financial support from Generalitat Valenciana
593 (project PROMETEO/2012/029) which is gratefully acknowledged. Besides, support from

594 FCC Aqualia participation in INNPRONTA 2011 IISIS IPT-20111023 project (partially
595 funded by The Centre for Industrial Technological Development (CDTI) and from the
596 Spanish Ministry of Economy and Competitiveness) is gratefully acknowledged.

597

598 **References**

- 599 APHA, 2005. Standard Methods for the Examination of Water and Wastewater. American
600 Public Health Association, Washington, DC.
- 601 Batstone, D.J., Puyol, D., Flores-Alsina, X., Rodríguez, J., 2015. Mathematical modelling of
602 anaerobic digestion processes: applications and future needs. *Rev. Environ. Sci.*
603 *Bio/Technology* 14, 595–613.
- 604 Becker, A.M., Yu, K., Stadler, L.B., Smith, A.L., 2017. Co-management of domestic
605 wastewater and food waste: A life cycle comparison of alternative food waste diversion
606 strategies. *Bioresour. Technol.* 223, 131–140.
- 607 Ben, A., Semmens, M., 2002. Membrane bioreactors for wastewater treatment and reuse: a
608 success story. *Water Sci. Technol.* 47, 1–5.
- 609 Busch, J., Cruse, A., Marquardt, W., 2007. Run-to-run control of membrane filtration
610 processes. *AIChE J.* 53, 2316–2328.
- 611 Campolongo, F., Cariboni, J., Saltelli, A., 2007. An effective screening design for sensitivity
612 analysis of large models. *Environ. Model. Softw.* 22, 1509–1518.
- 613 Capson-Tojo, G., Rouez, M., Crest, M., Steyer, J.-P., Delgenès, J.-P., Escudié, R., 2016. Food
614 waste valorization via anaerobic processes: a review. *Rev. Environ. Sci. Bio/Technology*
615 15, 499–547.
- 616 Capson-Tojo, G., Rouez, M., Crest, M., Trably, E., Steyer, J., Bernet, N., Delgenes, J.,
617 Escudié, R., 2017. Kinetic study of dry anaerobic co-digestion of food waste and
618 cardboard for methane production. *Waste Manag.* 69, 470–479.
- 619 Coleman, T.F., Li, Y., 1996. An interior trust region approach for nonlinear minimization
620 subject to bounds. *SIAM J. Optim.* 6, 418–445.
- 621 Coop, J.B., 2002. The COST Simulation Benchmark: Description and Simulator Manual.
622 Luxembourg.
- 623 Deng, L., Guo, W., Ngo, H.H., Zhang, H., Wang, J., Li, J., Xia, S., Wu, Y., 2016. Biofouling
624 and control approaches in membrane bioreactors. *Bioresour. Technol.* 221, 656–665.
- 625 Drews, A., Arellano-Garcia, H., Schöneberger, J., Schaller, J., Kraume, M., Wozny, G., 2007.
626 Improving the efficiency of membrane bioreactors by a novel model-based control of
627 membrane filtration, in: 17th European Symposium on Computer Aided Process
628 Engineering – ESCAPE. pp. 345–350.
- 629 Drews, A., Arellano-Garcia, H., Schöneberger, J., Schaller, J., Wozny, G., Kraume, M., 2009.
630 Model-based recognition of fouling mechanisms in membrane bioreactors. *Desalination*
631 236, 224–233.

- 632 Ferrero, G., Monclus, H., Buttiglieri, G., Comas, J., Rodriguez-Roda, I., 2011. Automatic
633 control system for energy optimization in membrane bioreactors. *Desalination* 268, 276–
634 280.
- 635 Ferrero, G., Monclus, H., Buttiglieri, G., Gabarron, S., Comas, J., Rodriguez-Roda, I., 2011.
636 Development of an algorithm for air-scour optimization in Membrane Bioreactors, IFAC
637 Proceedings Volumes (IFAC-PapersOnline). IFAC.
- 638 Ferrero, G., Monclús, H., Sancho, L., Garrido, J.M., Comas, J., Rodríguez-Roda, I., 2011. A
639 knowledge-based control system for air-scour optimisation in membrane bioreactors.
640 *Water Sci. Technol.* 63, 2025–2031.
- 641 Foscoliano, C., Del Vigo, S., Mulas, M., Tronci, S., 2016. Predictive control of an activated
642 sludge process for long term operation. *Chem. Eng. J.* 304, 1031-1044.
- 643 Gabarron, S., Ferrero, G., Dalmau, M., Comas, J., Rodriguez-Roda, I., 2014. Assessment of
644 energy-saving strategies and operational costs in full-scale membrane bioreactors. *J.*
645 *Environ. Manage.* 134, 8–14.
- 646 Gernaey, K. V, van Loosdrecht, M.C., Henze, M., Lind, M., Jørgensen, S.B., 2004. Activated
647 sludge wastewater treatment plant modelling and simulation: state of the art. *Environ.*
648 *Model. Softw.* 19, 763–783.
- 649 Giménez, J.B., Robles, A., Carretero, L., Durán, F., Ruano, M.V., Gatti M.N., Ribes, J.,
650 Ferrer, J., Seco, A., 2011. Experimental study of the anaerobic urban wastewater
651 treatment in a submerged hollow-fibre membrane bioreactor at pilot scale. *Bioresour.*
652 *Technol.* 102, 8799-8806.
- 653 Huyskens, C., Brauns, E., Van Hoof, E., Diels, L., De Wever, H., 2011. Validation of a
654 supervisory control system for energy savings in membrane bioreactors. *Water Res.* 45,
655 1443–1453.
- 656 Jeppsson, U., Rosen, C., Alex, J., Copp, J., Gernaey, K. V., Pons, M.N., Vanrolleghem, P. a.,
657 2006. Towards a benchmark simulation model for plant-wide control strategy
658 performance evaluation of WWTPs. *Water Sci. Technol.* 53, 287–295.
- 659 Jimenez, J., Latrille, E., Harmand, J., Robles, A., Ferrer, J., Gaida, D., Wolf, C., Mairet, F.,
660 Bernard, O., Alcaraz-Gonzalez, V., 2015. Instrumentation and control of anaerobic
661 digestion processes: a review and some research challenges. *Rev. Environ. Sci.*
662 *Bio/Technology* 14, 615–648.
- 663 Judd, S., Judd, C., 2011. *The MBR Book: Principles and applications of membrane*
664 *bioreactors for water and wastewater treatment*, 2nd ed. Elsevier, London (UK).
- 665 Kibler, K.M., Reinhart, D., Hawkins, C., Motlagh, A.M., Wright, J., 2018. Food waste and the
666 food-energy-water nexus: A review of food waste management alternatives. *Waste*
667 *Manag.*, In Press.
- 668 Maere, T., Verrecht, B., Moerenhout, S., Judd, S., Nopens, I., 2011. BSM-MBR: A
669 benchmark simulation model to compare control and operational strategies for
670 membrane bioreactors. *Water Res.* 45, 2181–2190.
- 671 Mannina, G., Cosenza, A., 2013. The fouling phenomenon in membrane bioreactors:
672 Assessment of different strategies for energy saving. *J. Memb. Sci.* 444, 332–344.
- 673 Martin, C., Vanrolleghem, P.A., 2014. Analysing, completing, and generating influent data
674 for WWTP modelling: A critical review. *Environ. Model. Softw.* 60, 188–201.

- 675 Moñino, P., Aguado, D., Barat, R., Jiménez, E., Giménez, J.B., Seco, A., Ferrer, J., 2017. A
676 new strategy to maximize organic matter valorization in municipalities: Combination of
677 urban wastewater with kitchen food waste and its treatment with AnMBR technology.
678 *Waste Manag.* 62, 274–289.
- 679 Moñino, P., Jiménez, E., Barat, R., Aguado, D., Seco, A., Ferrer, J., 2016. Potential use of the
680 organic fraction of municipal solid waste in anaerobic co-digestion with wastewater in
681 submerged anaerobic membrane technology. *Waste Manag.* 56, 158–165.
- 682 Morris, M., 1991. Factorial sampling plans for preliminary computational experiments.
683 *Technometrics* 33, 239–245.
- 684 Nguyen, D., Gadhamshetty, V., Nitayavardhana, S., Khanal, S.K., 2015. Automatic process
685 control in anaerobic digestion technology: A critical review. *Bioresour. Technol.* 193,
686 513–522.
- 687 Pianosi, F., Beven, K., Freer, J., Hall, J.W., Rougier, J., Stephenson, D.B., Wagener, T., 2016.
688 Sensitivity analysis of environmental models: A systematic review with practical
689 workflow. *Environ. Model. Softw.* 79, 214–232.
- 690 Pretel, R., Moñino, P., Robles, A., Ruano, M. V., Seco, A., Ferrer, J., 2016. Economic and
691 environmental sustainability of an AnMBR treating urban wastewater and organic
692 fraction of municipal solid waste. *J. Environ. Manage.* 179, 83–92.
- 693 Raskin, L., 2012. Anaerobic membrane bioreactors for sustainable wastewater treatment.
694 WERF report U4R08.
- 695 Robles, A., Duran, F., Ruano, M.V., Ribes, J., Rosado, A., Seco, A., Ferrer, J., 2015.
696 Instrumentation, control, and automation for submerged anaerobic membrane
697 bioreactors. *Environ. Technol.* 36, 1–12.
- 698 Robles, A., Ruano, M.V., Ribes, J., Ferrer, J., 2013a. Advanced control system for optimal
699 filtration in submerged anaerobic MBRs (SAnMBRs). *J. Memb. Sci.* 430, 330–341.
- 700 Robles, A., Ruano, M. V., Ribes, J., Ferrer, J., 2013b. Factors that affect the permeability of
701 commercial hollow-fibre membranes in a submerged anaerobic MBR (HF-SAnMBR)
702 system. *Water Res.* 47, 1277–1288.
- 703 Robles, A., Ruano, M. V., Ribes, J., Seco, A., Ferrer, J., 2013c. A filtration model applied to
704 submerged anaerobic MBRs (SAnMBRs). *J. Memb. Sci.* 444, 139–147.
- 705 Robles, A., Ruano, M. V., Ribes, J., Seco, A., Ferrer, J., 2013d. Mathematical modelling of
706 filtration in submerged anaerobic MBRs (SAnMBRs): Long-term validation. *J. Memb.*
707 *Sci.* 446, 303–309.
- 708 Robles, A., Ruano, M. V., Ribes, J., Seco, A., Ferrer, J., 2014a. Model-based automatic tuning
709 of a filtration control system for submerged anaerobic membrane bioreactors (AnMBR).
710 *J. Memb. Sci.* 465, 14–26.
- 711 Robles, A., Ruano, M. V., Ribes, J., Seco, A., Ferrer, J., 2014b. Global sensitivity analysis of
712 a filtration model for submerged anaerobic membrane bioreactors (AnMBR). *Bioresour.*
713 *Technol.* 158, 365–373.
- 714 Rojas, J.D., Flores-Alsina, X., Jeppsson, U., Vilanova, R., 2012. Application of multivariate
715 virtual reference feedback tuning for wastewater treatment plant control. *Control Eng.*
716 *Pract.* 20, 499–510.

- 717 Ruano, M.V., Ribes, J., Seco, A., Ferrer, J., 2012. An improved sampling strategy based on
718 trajectory design for application of the Morris method to systems with many input
719 factors. *Environ. Model. Softw.* 37, 103-109.
- 720 Saltelli, A., Chan, K., Scott, E.M., 2000. *Sensitivity Analysis*. John Wiley & Sons, New York.
- 721 Sheets, J.P., Yang, L., Ge, X., Wang, Z., Li, Y., 2015. Beyond land application: Emerging
722 technologies for the treatment and reuse of anaerobically digested agricultural and food
723 waste. *Waste Manag.* 44, 94-115.
- 724 Verrecht, B., Maere, T., Nopens, I., Brepols, C., Judd, S., 2010. The cost of a large-scale
725 hollow fibre MBR. *Water Res.* 44, 5274-5283.
- 726 Yang, M., Wei, Y., Zheng, X., Wang, F., Yuan, X., Liu, J., Luo, N., Xu, R., Yu, D., Fan, Y.,
727 2016. CFD simulation and optimization of membrane scouring and nitrogen removal for
728 an airlift external circulation membrane bioreactor. *Bioresour. Technol.* 219, 566-575.
- 729 Yang, M., Yu, D., Liu, M., Zheng, L., Zheng, X., Wei, Y., Wang, F., Fan, Y., 2017.
730 Optimization of MBR hydrodynamics for cake layer fouling control through CFD
731 simulation and RSM design. *Bioresour. Technol.* 227, 102-111.
- 732

733 **Figure captions**

734 **Figure 1.** (A) Sequence of the different operational stages in the membrane modules during
735 the alternative operating mode and (B) flow diagram of the proposed optimization
736 methodology

737 **Figure 2.** (A) Values of BRF and SRF and (B) t_F and t_{BF} optimized by the model-based
738 controller. The results were obtained using UWW as substrate

739 **Figure 3.** Evolution of the TMPs and different stages simulated. The results were obtained
740 using UWW as substrate

741 **Figure 4.** (A) Values of BRF and SRF and (B) t_F and t_{BF} optimized by the model-based
742 controller. The results were obtained using UWW and FW as substrates

743 **Figure 5.** Evolution of the energy requirements of the filtration process with the controller
744 operating at $17 \text{ g}\cdot\text{l}^{-1}$ MLTS entering the membrane tanks. The results for feeding strategies are
745 shown: (A) UWW and (B) mixture of UWW and FW

746 **Figure 6.** Evolution of the costs of the filtration process with the controller operating at $17 \text{ g}\cdot\text{l}^{-1}$
747 MLTS entering the membrane tanks. The results for feeding strategies are shown: (A) UWW
748 and (B) mixture of UWW and FW

749 **Table captions**

750 **Table 1.** Average values of the operational parameters evaluated in this study. The intervals
751 of uncertainty, as well as the initial values for the model-based controller (Monte Carlo
752 results) are also presented

753 **Table 2.** Sensitivity rankings for r_{opt} with UWW as substrate ($r_{opt} = 60$) and the mixture of
754 UWW and FW ($r_{opt} = 40$)

755 **Table 3.** Average energy requirements of the filtration process with the controller operating at
756 $17 \text{ g}\cdot\text{l}^{-1}$ MLTS entering the membrane tanks

757 **Table 4.** Average costs of the filtration process with the controller operating at $17 \text{ g}\cdot\text{l}^{-1}$ MLTS
758 entering the membrane tanks

759 **Supplementary material**

760 **Figure S1.** Net transmembrane flow (J_{net}) applied during the validation of the model-based
761 controller by simulation. The corresponding values of the MLTS concentrations in the
762 membrane tanks (MLTS_{MT}) during the co-digestion experiment at $17 \text{ g}\cdot\text{l}^{-1}$ are also shown

763 **Figure S2.** TMP simulated by the model (TMP_{sim}) vs experimental TMP (TMP_{exp})

764 Hierarchical clustering analysis based on the absolute means of the selected parameters with
765 UWW as substrate

766 **Figure S3.** Hierarchical clustering analysis based on the absolute means of the selected
767 parameters obtained (A) with (a) UWW as substrate and (B) with UWW and FW as substrates

768 **Figure S4.** Sensitivity measurements (μ^* and σ) obtained (A) with UWW as substrate (r_{opt} of
769 60) and (B) with the mixture of UWW and FW as substrate (r_{opt} of 40)

770 **Figure S5.** Correlation matrix ($\alpha = 0.05$; $n = 999$) of the optimized parameters, the energy
771 requirements and the filtration costs obtained (A) with UWW as substrate and (B) with
772 mixture of UWW and FW as substrate. The MLTS_{MT} , J_{net} and TMP are also included

773 **Table S1.** Average costs of filtration process and energy requirements with the controller
774 operating at 11, 13, 15 and $17 \text{ g}\cdot\text{l}^{-1}$ for both feeding strategies.

775

776

777

778

779

780

781

782

783

784 **Abbreviation and symbols**

785 **AeMBR** - Aerobic membrane bioreactor

786 **AnMBR** - Submerged anaerobic membrane bioreactor

787 **BRF** – Biogas recycling flow-rate

788 **BF** – Back-flushing period

789 **C_B** – Operating cost of membrane scouring by biogas sparging

790 **C_{LIFESPAN}** – Cost of membrane replacement due to irreversible fouling.

791 **C_{REAGENTS}** – Cost of reagents needed to clean irreversible fouling

792 **C_{SRF}** – Operating cost of pumping the sludge

793 **C_{STAGE}** – Operating cost of pumping permeate

794 **CT** – Control time

795 **C_{TOTAL}** – Total operating costs

796 **C_W** – Total energetic cost

797 **D** – Pipe diameter

798 **E_{COST}** – Cost of energy

799 **EE_i** – Elemental effects of each input factor on the model output

800 **f** – Number of filtration periods

801 **fr** – Friction factor

802 **F** – Filtration period

803 **f_{BF}** – Back-flush frequency

804 **F_i** – Scaled elementary effect distribution

805 **g** – Acceleration of gravity

806 **GSA** – Global sensitivity analysis

807 **HCA** – Hierarchical clustering analysis

808 **HRT** – Hydraulic retention time

- 809 **J_{BF}** – Transmembrane flow during back-flush
- 810 **J_{net}** – Net transmembrane flow
- 811 **L** – Pipe length
- 812 **L_{eq}** – Equivalent pipe length of accidental pressure drops
- 813 **M** – Molar flow rate of biogas
- 814 **MBR** - Membrane bioreactor
- 815 **MLTS** – Mixed liquor total solids
- 816 **$MLTS_{MT}$** – MLTS concentration in the membrane tanks
- 817 **OFMSW** - Organic fraction of municipal solid waste
- 818 **P_1** – Absolute inlet pressure
- 819 **P_2** – Absolute outlet pressure
- 820 **q** – Volumetric flow rate
- 821 **R** – Relaxation period
- 822 **R_g** – Ideal gas constant
- 823 **R_C** – Resistance of the solid cake formed on the surface of the membrane
- 824 **R_I** – Resistance due to irreversible fouling of the membrane
- 825 **R_M** – Resistance intrinsic to the membrane
- 826 **r_{opt}** – Optimum number of times that the SEE_i should be calculated
- 827 **R_T** – Total filtration resistance
- 828 **SEE_i** – Scaled elementary effect
- 829 **SDG_m** – Specific demand of gas per square meter of membrane
- 830 **SRF** – Sludge recycling flow-rate
- 831 **SRT** – Solids retention time
- 832 **t_{BF}** – Duration of the back-flushing stage
- 833 **t_F** – Duration of the filtration stage

- 834 T_{gas} – Biogas temperature
- 835 TMP – Transmembrane pressure
- 836 TMP_{sim} – Simulated transmembrane pressure
- 837 TMP_{exp} – Experimental transmembrane pressure
- 838 TS – Total solids
- 839 t_{R} – Duration of the relaxation stage
- 840 UWW - Urban wastewater
- 841 \mathbf{V} – Fluid velocity
- 842 \mathbf{V}_{T} – Net volume of treated wastewater
- 843 $\mathbf{W}_{\text{back-flushing}}$ – Energy requirements of the back-flushing pump
- 844 \mathbf{W}_{BRF} – Energy requirements of the biogas lower
- 845 $\mathbf{W}_{\text{filtration}}$ – Energy requirements of the permeate filtration pump
- 846 \mathbf{W}_{SRF} – Energy requirements of the sludge recycling pump
- 847 \mathbf{X}_{mC} – Dry mass of cake in the membrane surface
- 848 \mathbf{X}_{mI} – Dry mass of irreversible fouling on the membrane surface
- 849 \mathbf{X}_{TS} – Concentration of total solids in the mixed liquor
- 850 $\mathbf{Z}_1\text{-}\mathbf{Z}_2$ – difference in height
- 851 α – Compression index
- 852 α_{C} – Average specific resistance of the solid cake
- 853 α_{I} – Average specific resistance of the irreversible fouling
- 854 σ – Standard deviation
- 855 ρ_{sludge} – sludge density
- 856 η_{blower} – Overall mechanical and electrical efficiency of the blower
- 857 η_{pump} – Overall mechanical and electrical efficiency of the pump
- 858 μ – Mean

- 859 μ^* – Absolute mean (μ^*)
- 860 μ_p – Dynamic viscosity of the permeate
- 861 ω_C – Mass of solids settled per membrane area
- 862 ω_I – Mass of irreversible fouling per membrane area
- 863 $\Delta R_{I,MAX}$ – Upper threshold of irreversible fouling resistance at which membrane cleaning
- 864 starts
- 865

Graphical abstract

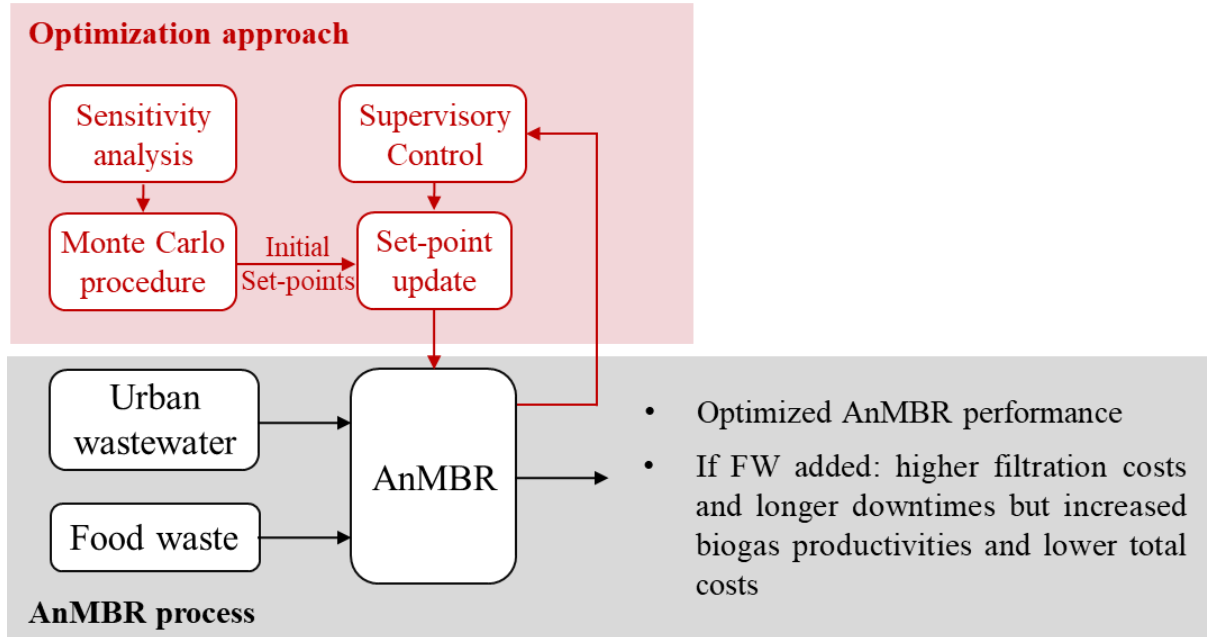


Table 1. Average values of the operational parameters evaluated in this study. The intervals of uncertainty, as well as the initial values for the model-based controller (Monte Carlo results) are also presented

Parameter	Units	Substrate	Average values	Minimum	Maximum	Monte Carlo results
BRF	$\text{m}^3 \cdot \text{h}^{-1}$	$\frac{\text{UWW}}{\text{UWW} + \text{FW}}$	12	3	21	13
		$\frac{\text{UWW}}{\text{UWW} + \text{FW}}$	12	3	21	13
SRF	$\text{m}^3 \cdot \text{h}^{-1}$	$\frac{\text{UWW}}{\text{UWW} + \text{FW}}$	2.1	1.5	2.7	2.0
		$\frac{\text{UWW}}{\text{UWW} + \text{FW}}$	2.1	1.5	2.7	1.8
t_F	s	$\frac{\text{UWW}}{\text{UWW} + \text{FW}}$	400	200	600	600
		$\frac{\text{UWW}}{\text{UWW} + \text{FW}}$	400	200	600	485
t_R	s	$\frac{\text{UWW}}{\text{UWW} + \text{FW}}$	35	10	60	10
		$\frac{\text{UWW}}{\text{UWW} + \text{FW}}$	35	10	60	10
t_{BF}	s	$\frac{\text{UWW}}{\text{UWW} + \text{FW}}$	35	10	60	17
		$\frac{\text{UWW}}{\text{UWW} + \text{FW}}$	35	10	60	31
f_{BF}	-	$\frac{\text{UWW}}{\text{UWW} + \text{FW}}$	11	1	21	10
		$\frac{\text{UWW}}{\text{UWW} + \text{FW}}$	11	1	21	4
J_{BF}	LMH	$\frac{\text{UWW}}{\text{UWW} + \text{FW}}$	15	10	20	16
		$\frac{\text{UWW}}{\text{UWW} + \text{FW}}$	15	10	20	10

Table 2. Sensitivity rankings for r_{opt} with UWW as substrate ($r_{\text{opt}} = 60$) and the mixture of UWW and FW ($r_{\text{opt}} = 40$)

UWW			UWW + FW		
Parameter	μ^*	σ	Parameter	μ^*	σ
BRF	1.253	1.856	BRF	1.355	2.099
f_{BF}	0.770	2.220	f_{BF}	0.579	1.418
t_F	0.724	1.921	t_{BF}	0.344	1.059
t_{BF}	0.574	1.210	t_F	0.252	0.710
SRF	0.464	1.584	SRF	0.163	0.410
t_R	0.057	0.261	t_R	0.067	0.138
J_{BF}	0.057	0.268	J_{BF}	0.005	0.018

Table 3. Average energy requirements of the filtration process with the controller operating at 17 g·l⁻¹ MLTS entering the membrane tanks

Substrate	W_{TOTAL} (kWh·m ⁻³)	W_{BRF} (%)	W_{SRF} (%)	W_{Stage} (%)
UWW	0.20	79.7	16.9	14.3
UWW + FW	0.34	88.5	9.6	9.8

Table 4. Average costs of the filtration process with the controller operating at $17 \text{ g}\cdot\text{l}^{-1}$ MLTS entering the membrane tanks

Substrate	C_{TOTAL} (€ per m³)	C_W (%)	C_{REAGENTS} (%)	C_{LIFESPAN} (%)
UWW	0.047	59.6	17.0	23.4
UWW + FW	0.067	69.0	13.0	18.0

Figure 1

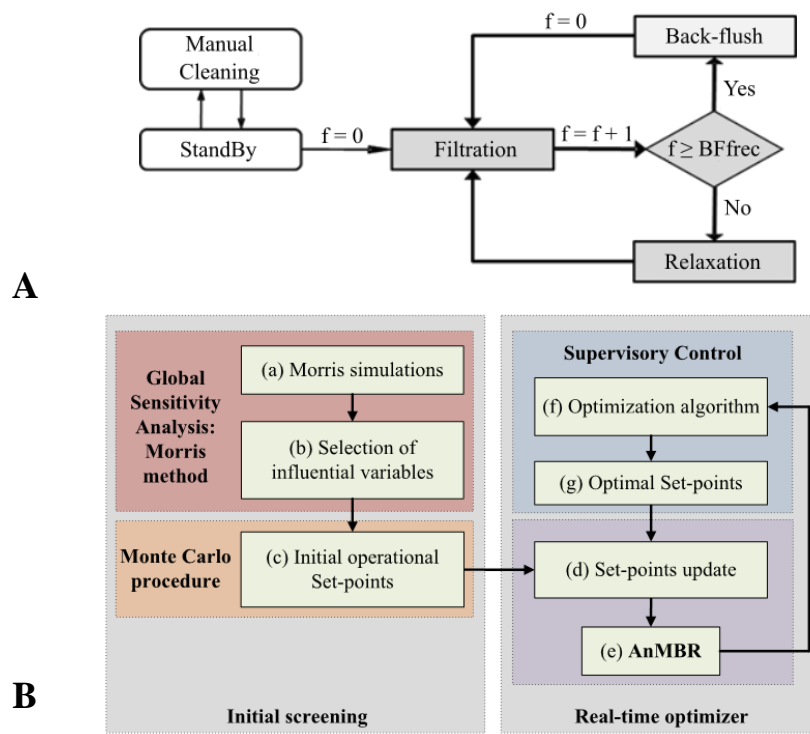


Figure 1. (A) Sequence of the different operational stages in the membrane modules during the alternative operating mode and (B) flow diagram of the proposed optimization methodology

Figure 2

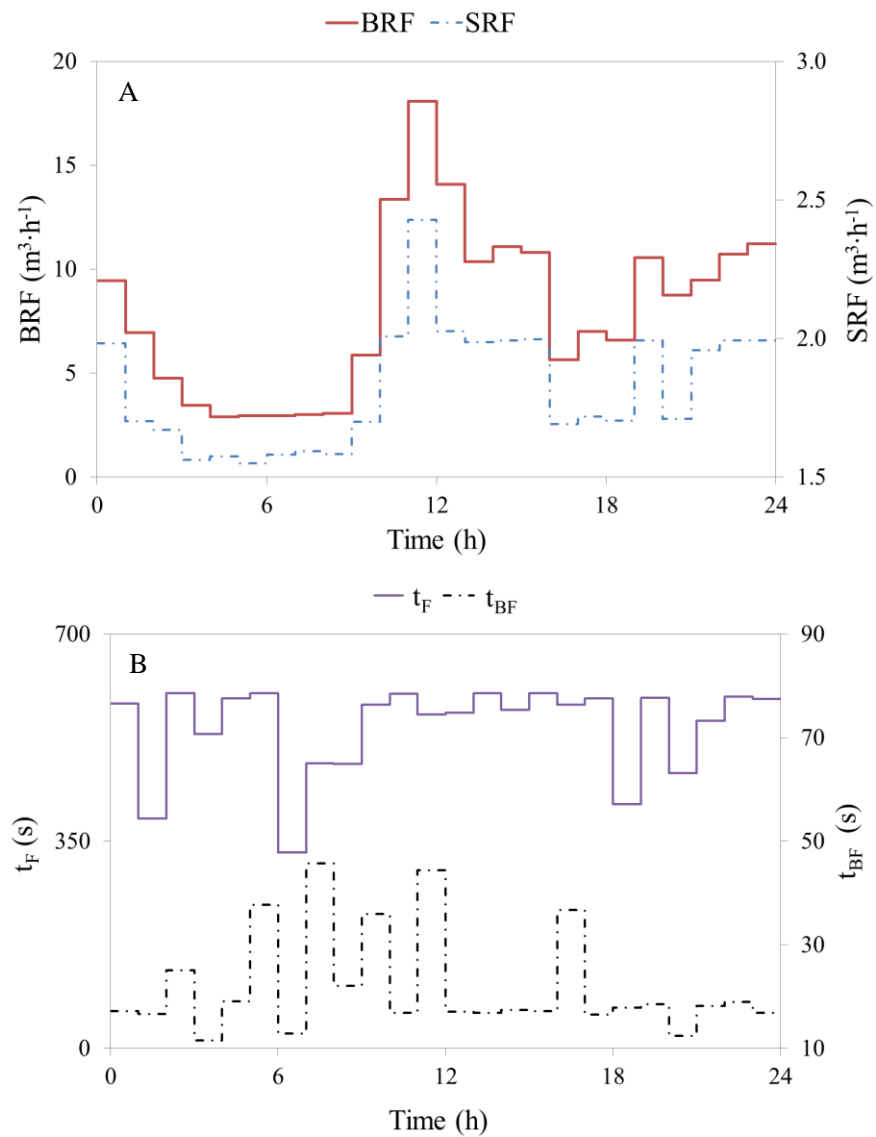


Figure 2. (A) Values of BRF and SRF and (B) t_F and t_{BF} optimized by the model-based controller. The results were obtained by applying the transmembrane flux shown in Figure S1 with a MLTS concentration entering the tanks of $17 \text{ g} \cdot \text{l}^{-1}$ and using UWW as substrate

Figure 3

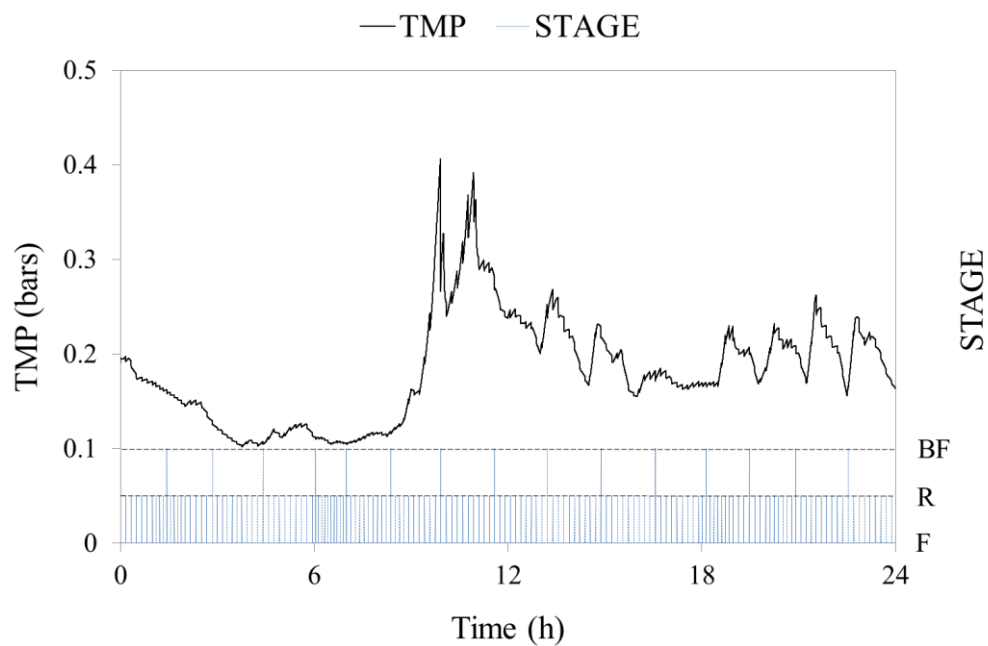


Figure 3. Evolution of the TMPs and different stages simulated. The results were obtained by applying the transmembrane flux shown in Figure S1 with a MLTS concentration entering the tanks of $17 \text{ g}\cdot\text{l}^{-1}$ and using UWW as substrate

Figure 4

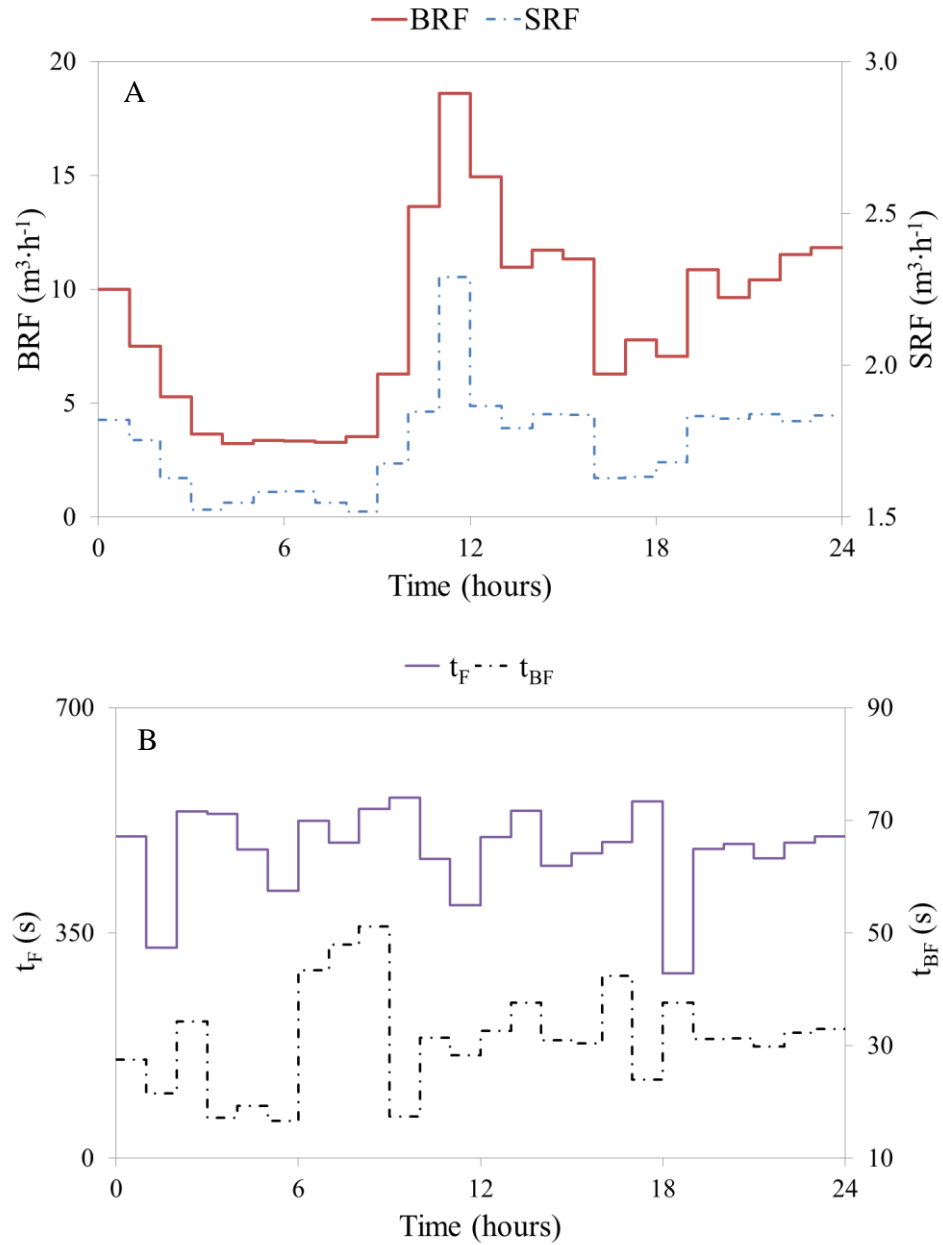


Figure 4. (A) Values of BRF and SRF and (B) t_F and t_{BF} optimized by the model-based controller. The results were obtained by applying the transmembrane flux shown in Figure S1 with a MLTS concentration entering the tanks of $17 \text{ g} \cdot \text{l}^{-1}$ and using UWW and FW as substrates

Figure 5

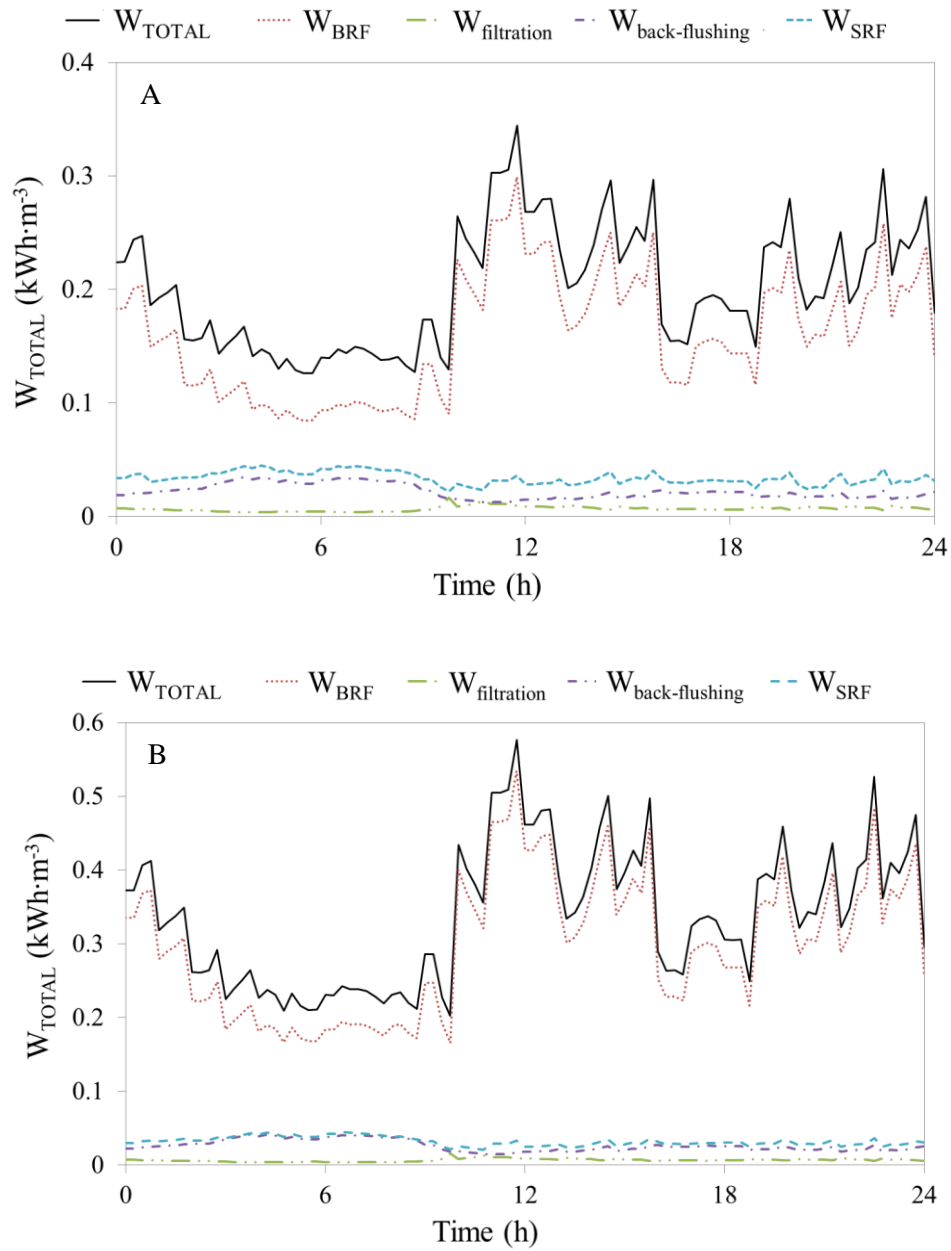


Figure 5. Evolution of the energy requirements of the filtration process with the controller operating at $17 \text{ g}\cdot\text{l}^{-1}$ MLTS entering the membrane tanks. The results for feeding strategies are shown: (A) UWW and (B) mixture of UWW and FW

Figure 6

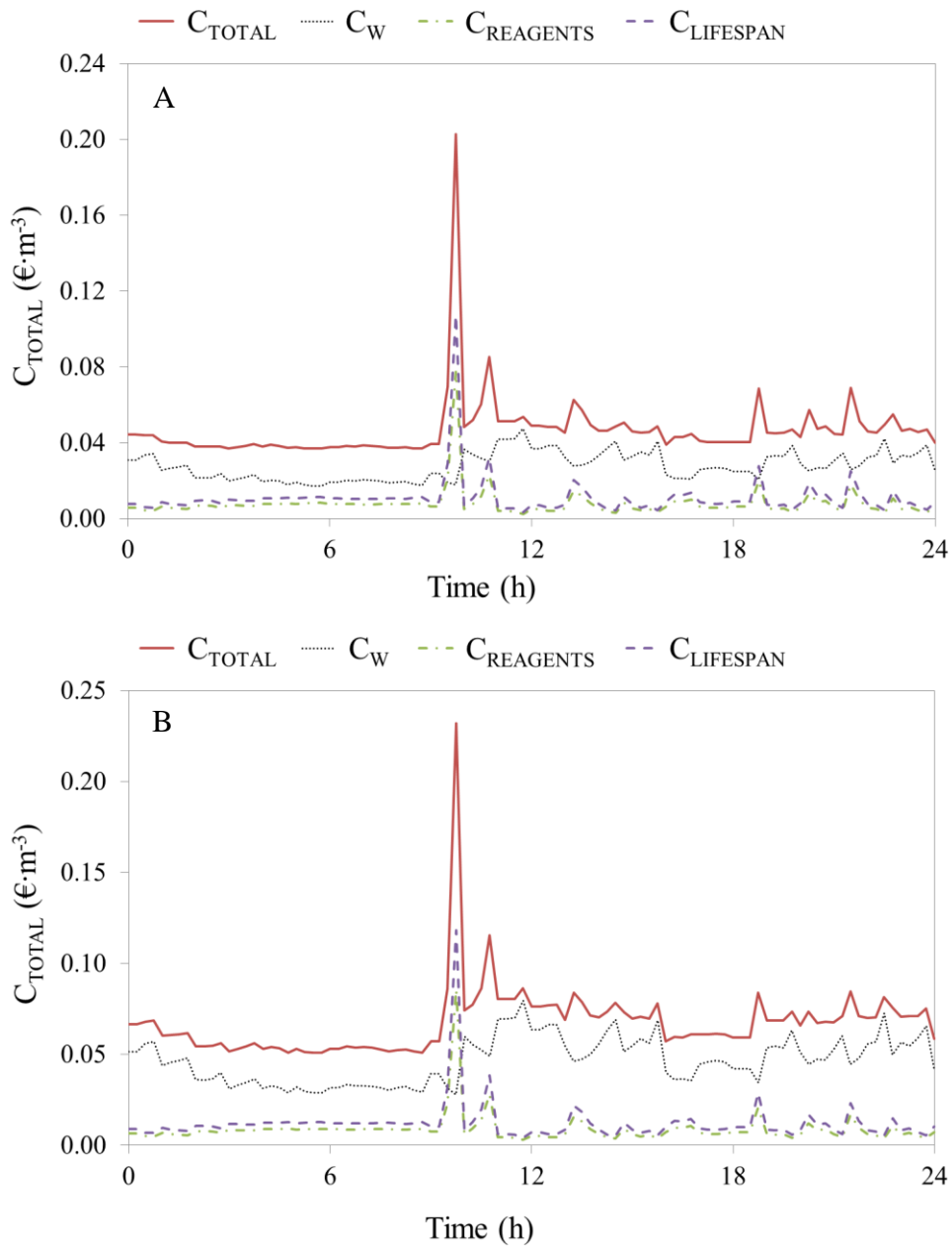


Figure 6. Evolution of the costs of the filtration process with the controller operating at $17 \text{ g}\cdot\text{l}^{-1}$ MLTS entering the membrane tanks. The results for feeding strategies are shown: (A) UWW and (B) mixture of UWW and FW

Figure S1

[Click here to download E-Component: Figure S1.docx](#)

Figure S2

[Click here to download E-Component: Figure S2.docx](#)

Figure S3

[Click here to download E-Component: Figure S3.docx](#)

Figure S4

[Click here to download E-Component: Figure S4.docx](#)

Figure S5

[Click here to download E-Component: Figure S5.docx](#)

Table S1

[Click here to download E-Component: Table S1.docx](#)